New Electrocatalysts for the Four-Electron Reduction of Dioxygen Based on (5,10,15-Tris(pentaammineruthenium(II)-4-cyanophenyl)-20-(1-methylpyridinium-4-yl)porphyrinato)cobalt(II) Immobilized on Graphite Electrodes†

Beat Steiger and Fred C. Anson*

Arthur Amos Noyes Laboratories, Division of Chemistry and Chemical Engineering, California Institute of Technology, Pasadena, California 91125

Received July 1, 1994®

Coordination of $Ru(NH_3)_5^{2+}$ centers to the nitrile sites in (5,10,15-tris(4-cyanophenyl)-20-(1-methylpyridinium-4-yl)porphyrinato)cobalt(II) immobilized on pyrolytic graphite electrodes produces the triruthenated complex which acts as an electrocatalyst for the four-electron reduction of dioxygen to water. For comparison, $Ru(NH_3)_5^{2+}$ centers were also coordinated to the nitrile sites in (5,10-bis(4-cyanophenyl)-15,20-bis(1-methylpyridinium-4-yl)porphyrinato)cobalt(II), (5,15-bis(4-cyanophenyl)-10,20-bis(1-methylpyridinium-4-yl)porphyrinato)cobalt(II) and (5-(4-cyanophenyl)-10,15,20-tris(1-methylpyridinium-4-yl)porphyrinato)cobalt(II) to produce the corresponding di- and monoruthenated complexes. The diruthenated complexes exhibit some electrocatalytic activity for the four-electron reduction of dioxygen, whereas the monoruthenated complex catalyzes only the two-electron reduction to hydrogen peroxide. None of the ruthenated cobalt porphyrins are catalysts for the reduction of hydrogen peroxide. The synthesis and the electrocatalytic behavior of the set of structurally related porphyrins are described. It is argued that the ruthenated porphyrins achieve their catalytic activity for the reduction of dioxygen to water by means of back-bonding interactions between the $Ru(NH_3)_5^{2+}$ groups and the cobalt center of the porphyrin ring.

Introduction

In recent reports it has been demonstrated that the coordination of four $Ru(NH_3)_5^{2+}$ groups to the pyridine sites of (5,10,15,20-tetrakis(4-pyridyl)porphyrinato)cobalt(II) ($CoP(py)_4$) on electrode surfaces converts the complex from a two- to a four-electron catalyst for the electroreduction of O_2.[1,2] Related cobalt porphyrins containing combinations of 4-pyridyl or phenyl groups, $CoP(Ph)_x(py)_y$ (Ph = phenyl; $x + y = 4$; $y = 1$, 2, 3, 4) behaved as catalysts for the two-electron reduction of O_2 following coordination of $Ru(NH_3)_5^{2+}$ groups to the available pyridine sites when $y = 1$ or 2 but were converted to four-electron catalysts when $y = 3$ or 4.[3] Four-electron reduction catalysts were also fashioned from combinations of $CoP(py)_4$ and coordinated $Ru(NH_3)_3(OH_2)_x^{2+}$ groups ($x = 1$, 2)[4] but coordination of four $Ru(edta)^{2-}$ (edta = ethylenediaminetetraacetate) groups to $CoP(py)_4$ resulted in no change in catalytic activity: only the two-electron reduction of O_2 was observed.[3]

In continuing efforts to identify the factors that are important in the conversion of cobalt porphyrins from two-electron to four-electron catalysts for the reduction of O_2 by ruthenation of peripheral ligands on the porphyrin ring, we prepared a set of cobalt porphyrins containing various combinations of *N*-methylpyridinium-4-yl (*N*-CH_3py) and 4-cyanophenyl groups as peripheral ligands. The 4-cyanophenyl ligands were used to coordinate $Ru(NH_3)_5^{2+}$ groups to the porphyrin ring and the resulting complexes, confined to the surface of pyrolytic graphite electrodes, were tested as electrocatalysts during the reduction of O_2. Certain of the ruthenated cobalt porphyrins exhibited notable catalytic activity and accomplished the reduction of O_2 to H_2O. The preparation of these new cobalt porphyrins, their behavior as electrocatalysts and some suggestions about the mechanisms by which they operate are described in this report.

Results and Discussion

Syntheses. For reasons that are explained in what follows, it proved desirable to utilize cobalt porphyrins containing mixtures of 4-cyanophenyl and *N*-methylpyridinium-4-yl (*N*-CH_3py) groups as peripheral ligands. To obtain the desired porphyrins, the molecules shown in Figure 1 were prepared by a variation of a procedure utilized in our recent report[3] (see the Experimental Section). The porphyrins containing pyridyl groups were then converted to the corresponding *N*-CH_3py derivates and isolated as PF_6^- salts as described in the Experimental Section.

The identities of the products resulting from the syntheses were established from their ^1H NMR spectra. The *N*-CH_3py substituents exhibited the expected *N*-methyl-H resonance[5] and produced typical downfield shifts in the pyridyl-H resonances[5] (see the Experimental Section). The more complex spectra of the porphyrins with the two types of substituents were assignable on the basis of previously published spectra of analogous asymmetrically substituted porphyrins.[5,6] No evidence for methylation of the pyrrolic nitrogen atoms of the porphyrins was present in the spectra of the porphyrins containing the *N*-CH_3py groups[7,8] in agreement with the report of Pasternack and co-workers.[9]

Cobalt(II) was incorporated into each of the isolated porphyrins by standard methods[10] to produce the cobalt(II) porphyrins shown in Figure 2 and the resulting cobalt porphyrins were adsorbed on the surface of pyrolytic graphite electrodes to be ruthenated in place by reaction with $Ru(NH_3)_5OH_2^{2+}$ as in our

† Contribution No. 8963.
® Abstract published in *Advance ACS Abstracts,* November 1, 1994.

(1) Shi, C.; Anson, F. C. *J. Am. Chem. Soc.* **1991**, *113*, 9564.
(2) Shi, C.; Anson, F. C. *Inorg. Chem.* **1992**, *31*, 5078.
(3) Steiger, B.; Shi, C.; Anson, F. C. *Inorg. Chem.* **1993**, *32*, 2107
(4) Shi, C.; Anson, F. C. *Inorg. Chim. Acta* **1994**, *225*, 215.
(5) Czuchajowski, L.; Habdas, J.; Niedbala, H.; Wandrekar, V. *J. Heterocycl. Chem.* **1992**, *29*, 479.
(6) Walker, F. A.; Balke, V. L.; McDermott, G. A. *Inorg. Chem.* **1982**, *21*, 3342.

0020-1669/94/1333-5767$04.50/0

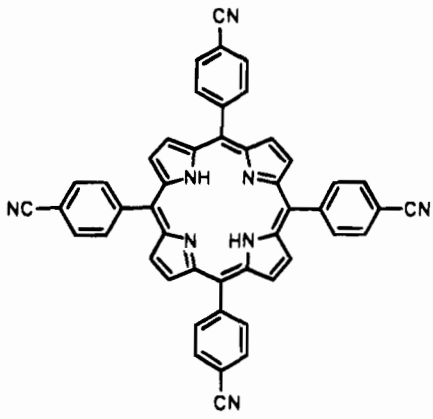

$H_2P(PhCN)_4$

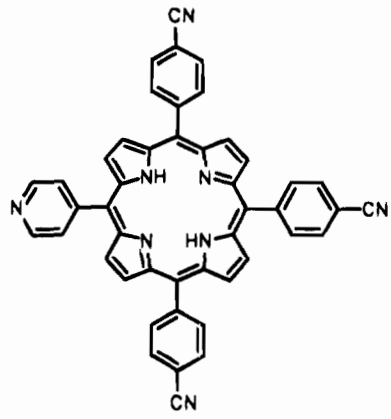

$H_2P(PhCN)_3(py)$

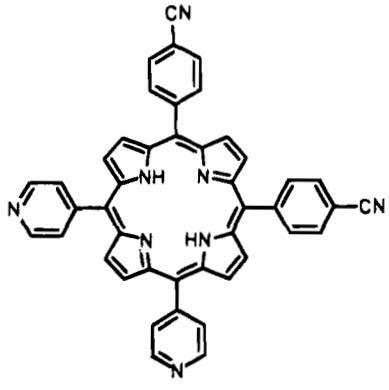

cis-$H_2P(PhCN)_2(py)_2$

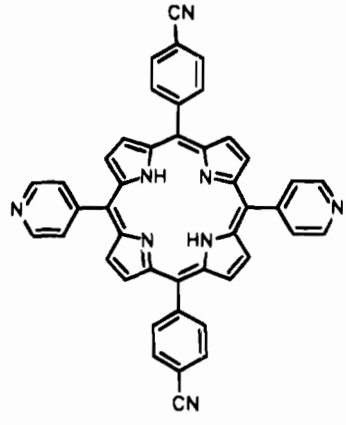

trans-$H_2P(PhCN)_2(py)_2$

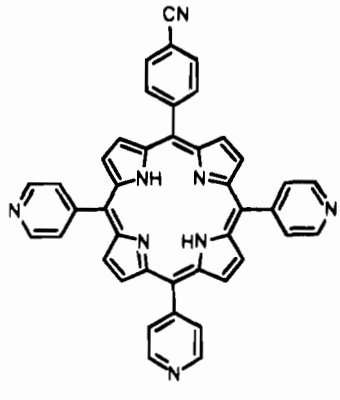

$H_2P(PhCN)(py)_3$

Figure 1. Structures of the metal-free porphyrins examined in this study with the abbreviations used for them in the text.

previous study with pyridyl porphyrins.[3] However, the present cobalt porphyrins did not remain on the graphite surfaces for sufficiently long times to complete the ruthenation reactions. It was, therefore, necessary to mix the porphyrins with a dilute alcoholic solution of Nafion before applying them to the electrode surfaces to obtain coatings which were retained on the graphite surface (see the Experimental section). Exposure of the resulting electrodes to solutions of $Ru(NH_3)_5OH_2^{2+}$ produced stable electrode coatings consisting of the ruthenated cobalt porphyrins shown in Figure 3.

Voltammetry of the Adsorbed Cobalt Porphyrins before Ruthenation. The voltammetric responses exhibited by the Co(III)/Co(II) couple of most cobalt porphyrins in aqueous media are ill-defined and difficult to identify. Such was the case with the $CoP(py)_4$ and the $CoP(Ph)_x(py)_y$ ($x + y = 4$; $x = 1, 2, 3$) porphyrins that were adsorbed on graphite and examined in our previous studies.[2,3] Adsorbed $CoP(PhCN)_4$ behaves similarly. A cyclic voltammogram for the latter complex adsorbed on graphite is shown in Figure 4A. Surprisingly, a

(7) Lavallee, D. K.; Gebala, A. E. *Inorg. Chem.* **1974**, *13*, 2004.
(8) Al-Hazimi, H. M. G.; Jackson, A. H.; Johnson, A. W.; Winter, M. *J. Chem. Soc., Perkin Trans. 1* **1977**, 98.
(9) Pasternack, R. F.; Huber, P. R.; Boyd, P.; Engasser, G.; Francesconi, L.; Gibbs, E.; Fasella, P.; Venturo, G. C.; Hinds, L. deC. *J. Am. Chem. Soc.* **1972**, *94*, 4511.
(10) Adler, A. D.; Longo, F. R.; Kampas, F.; Kim, J. *Inorg. Nucl. Chem.* **1970**, *32*, 2443.

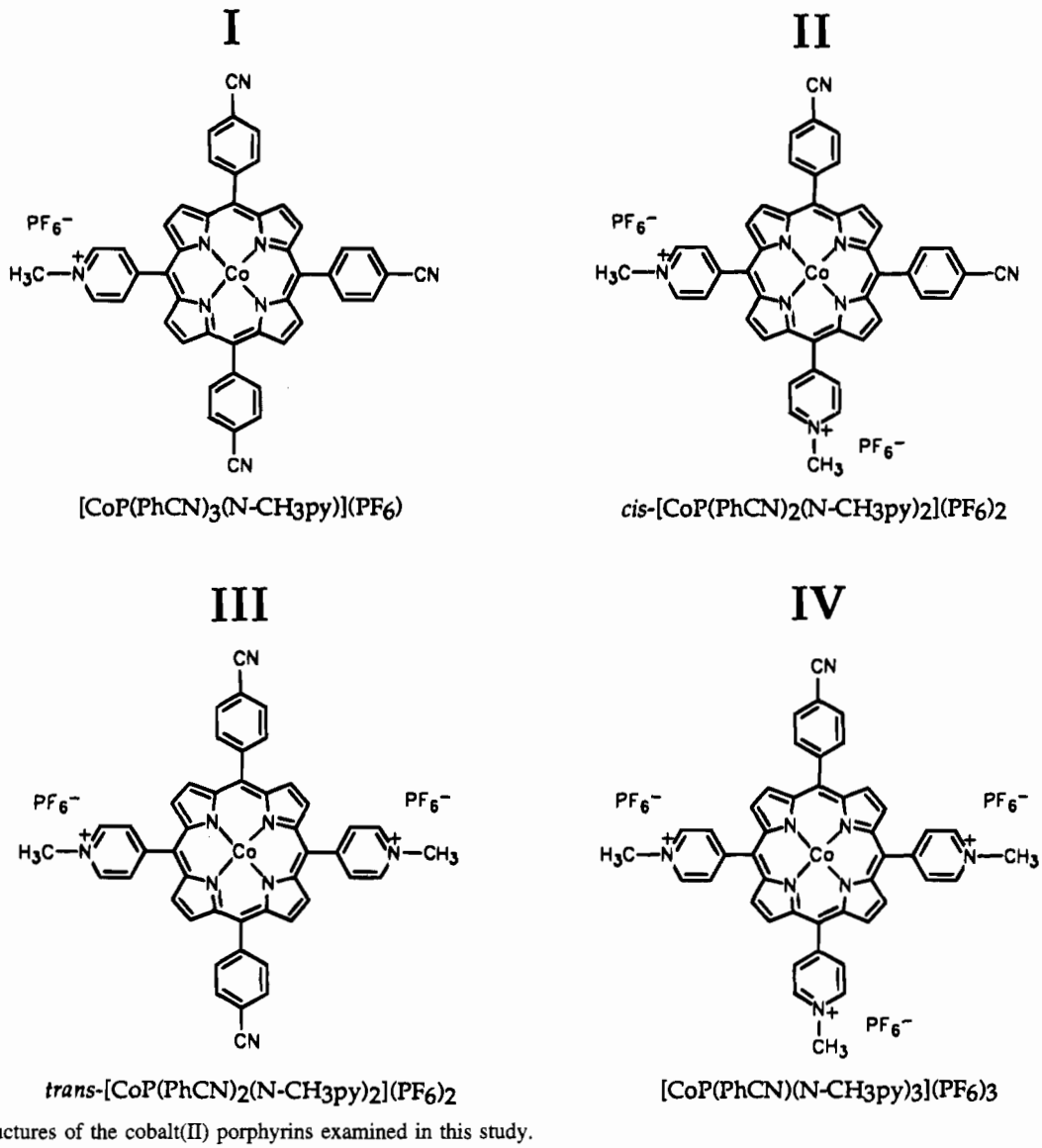

Figure 2. Structures of the cobalt(II) porphyrins examined in this study.

much better-defined response resulted from coatings of porphyrin I of Figure 2 as shown in Figure 4B. The area lying between the dashed and solid lines of the cathodic peaks in the voltammogram in Figure 4B corresponds to 1.2×10^{-9} mol cm^{-2} of adsorbed porphyrin compared with the 1.3×10^{-9} mol cm^{-2} that were dissolved in the aliquot of the standard solution of porphyrin I that was transferred to the electrode surface to prepare the coating. This reasonable agreement demonstrates that essentially all of the cobalt centers in the adsorbed porphyrin contribute to the voltammetric response. (The corresponding measurement with Figure 4A indicated that only 15% of the total cobalt porphyrin deposited on the electrode surface contributed to the broad cathodic peak.) When the coating containing the same amount of I was prepared from the cobalt porphyrin–Nafion mixture, the cathodic response became broader but a clear anodic peak remained (Figure 4C) with an area corresponding to that expected for the total quantity of cobalt porphyrin in the aliquot of the standard solution which was evaporated on the electrode surface. The results shown in Figure 4B and 4C showed that essentially all of the porphyrin deposited on the electrode surface remained on this surface when the electrode was immersed in the supporting electrolyte solution. The quantities of porphyrin present on the electrode surfaces were therefore determined either by measuring the areas of cyclic voltammograms or from the volumes of the standard porphyrin solutions transferred to the electrode surfaces.

With the more highly charged cobalt porphyrins, II, III and IV in Figure 2, no significant voltammetric peaks were obtained from porphyrin–Nafion coatings. We believe this behavior is a reflection of the strong association of the more highly charged complexes with the sulfonate groups of the Nafion present in the coatings. The stronger binding greatly diminishes the rates with which the porphyrins can move from the interior of the Nafion polyelectrolyte to the electrode surface to be oxidized or reduced. For these porphyrins, the quantities contained in the coatings were estimated from the volumes of the standard solutions transferred to the electrode surfaces.

As noted in the Experimental Section, to obtain coatings in which all of the cobalt centers were electroactive it was necessary to transfer the porphyrin solutions to the electrode surface in a series of small aliquots each of which was allowed to evaporate before the next was applied. When the same quantity of porphyrin was transferred in a single aliquot the porphyrin deposits appeared to be less solvated which diminished the voltammetric response from the Co(III)/Co(II) couple.

The reason that the presence of the *N*-CH_3py group on the porphyrin ring converts a negligible voltammetric response to the reasonably well formed peaks in Figures 4B and 4C may also involve the degree of solvation of the porphyrins in the coatings. The oxidation of the Co(II) centers to Co(III) requires that suitable axial ligands have access to the cobalt centers and

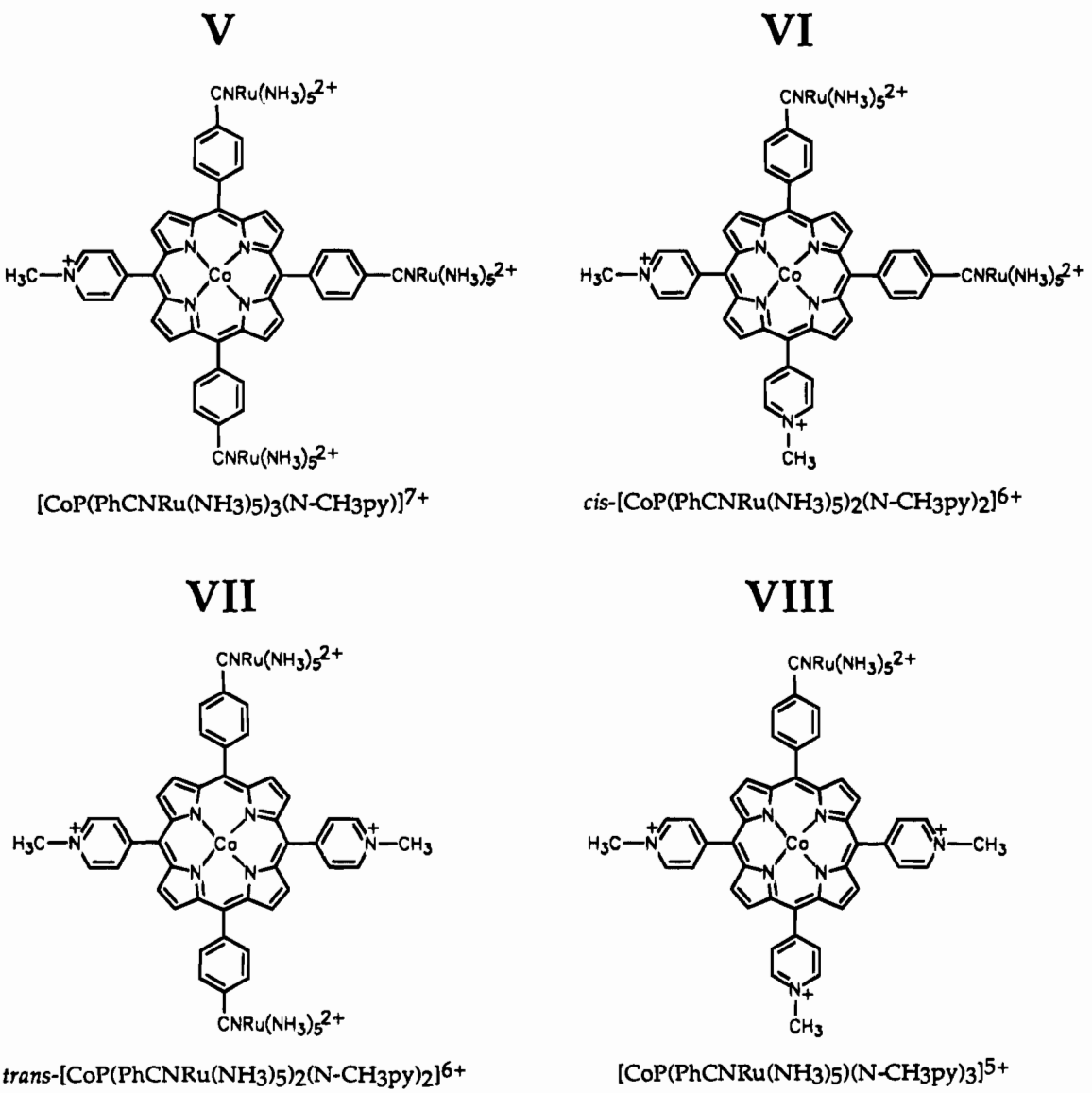

Figure 3. Structures of the ruthenated cobalt(II) porphyrins examined in this study.

such access is likely to be facilitated by the solvation of the porphyrin complexes which is induced by the charged *N*-CH_3py groups.

Voltammetry of the Adsorbed Cobalt Porphyrins after Ruthenation. To coordinate $Ru(NH_3)_5^{2+}$ complexes to the cobalt porphyrins in the coatings on the electrode surface, the electrodes were immersed in a 25 mM solution of $Ru(NH_3)_5OH_2^{2+}$. After various reaction times the electrodes were transferred to a ruthenium-free supporting electrolyte where cyclic voltammograms were recorded. The electrodes were then returned to the solution of $Ru(NH_3)_5OH_2^{2+}$ to allow the coordination of additional $Ru(NH_3)_5^{2+}$ groups to proceed. This process was continued until the voltammetric peak current corresponding to the $Ru(NH_3)_5(NCPh)^{3+/2+}$ couple reached its maximum value. A typical example of the cyclic voltammograms obtained during a ruthenation experiment is shown in Figure 5A. The dotted line shows the voltammetric response obtained at the uncoated graphite electrode. The dashed curve was obtained after the cobalt porphyrin−Nafion mixture was deposited on the electrode surface and the alcoholic solvent was allowed to evaporate at room temperature. The small peak currents from the Co(III)/Co(II) couple of the porphyrin can be seen. The solid curves were recorded after the coating was reacted with $Ru(NH_3)_5OH_2^{2+}$ for increasing times. The reversible couple with a formal potential of 0.28 V clearly corresponds to the Ru(III)/Ru(II) couple in the $Ru(NH_3)_5(NCPh)^{2+}$ complexes formed by the reaction of the porphyrin on the electrode surface with the $Ru(NH_3)_5OH_2^{2+}$ ions in solution. Previously reported formal potentials of the $Ru(NH_3)_5(NCPh)^{3+/2+}$ couple in solutions of this complex are 0.27 V in 0.1 M HCl[11] and 0.24 V in 0.1 M *p*-toluenesulfonate−0.1 M *p*-toluene sulfonic acid.[12] We observed a value of 0.22 V for the complex incorporated in Nafion with 0.5 M NH_4PF_6−0.5 M $HClO_4$ as supporting electrolyte. The small peak near −0.15 V in Figure 5A corresponds to the $Ru(NH_3)_5OH_2^{3+/2+}$ couple. It arises from the $Ru(NH_3)_5OH_2^{2+}$ that is incorporated by cation exchange into the Nafion present in the coating. This peak is small because much of the incorporated complex was removed from the Nafion by reverse ion-exchange before the voltammograms were recorded. The peak was eliminated entirely when the coated electrodes were held at −0.4 V and rotated at 100 rpm for a few minutes in the pure supporting electrolyte. Shown in Figure 5B is the final response obtained after removal of the uncoordinated $Ru(NH_3)_5OH_2^{2+}$ from the coating. The variation of the voltammetric response with the potential scan rate is shown in Figure 5C. The linear dependence of the peak currents on scan rate (Figure 5D) is the expected behavior for a reactant confined

(11) Diamond, S. E.; Tom, G. M.; Taube, H. *J. Am. Chem. Soc.* **1975**, *97*, 2661.
(12) Matsubara, T.; Ford, P. C. *Inorg. Chem.* **1976**, *15*, 1107.

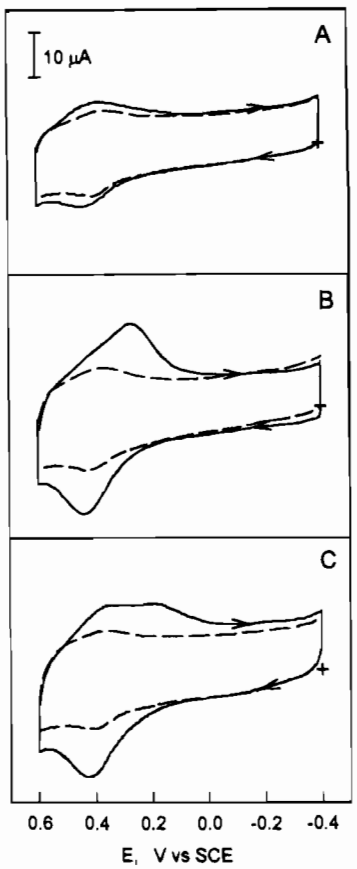

Figure 4. Cyclic voltammetry of cobalt(II) porphyrins confined on the surface of pyrolytic graphite electrodes. (A) 1.5×10^{-9} mol cm^{-2} of adsorbed $CoP(PhCN)_4$; (B) 1.2×10^{-9} mol cm^{-2} of adsorbed porphyrin I (Figure 2); (C) 2.1×10^{-9} mol cm^{-2} of porphyrin I plus Nafion (1.8×10^{-8} mol cm^{-2} of sulfonate groups). Supporting electrolyte: 0.5 M NH_4PF_6–0.5 M $HClO_4$ saturated with Ar. The dashed curves were recorded with bare (A, B) or Nafion-coated (C) electrodes. Scan rate = 50 mV s^{-1}.

to the electrode surface. The coulometric areas of the voltammograms in Figure 5C are independent of scan rate, as expected.

The area defined by the cathodic peak in Figure 5B (after subtraction of the area under the dashed curve in Figure 5A) was used to evaluate the quantity of $Ru(NH_3)_5(NCPh)$ groups present in the coating. A value of 6.1×10^{-9} mol cm^{-2} was obtained. The quantity of cobalt porphyrin present in the coating was 2.1×10^{-9} mol cm^{-2}. The ratio of 2.9 $Ru(NH_3)_5^{2+}$ centers per cobalt porphyrin showed that the ruthenation of the three nitrile ligands on each porphyrin molecule was essentially quantitative so that all of the molecules of I in the electrode coating were converted into the ruthenated porphyrin V shown in Figure 3. The voltammetric response from the ruthenated coating was stable for several hours in a supporting electrolyte consisting of 0.5 M NH_4PF_6–0.5 M $HClO_4$. The PF_6^- anions were needed to inhibit the dissolution of the ruthenated porphyrins into the electrolyte as previously noted.[2]

As was true of the multiply-ruthenated pyridyl porphyrins described previously,[3] the triply-ruthenated porphyrin V (Figure 3) exhibited only a single voltammetric peak with a formal potential corresponding to the $Ru(NH_3)_5(NCPh)^{3+/2+}$ couple. The three ruthenium complexes coordinated to each porphyrin molecule evidently interact with each other too weakly to produce a splitting of the $Ru^{3+/2+}$ response into separated couples with differing formal potentials. Behavior similar to that shown in Figure 5 was also obtained with coatings containing porphyrins VI, VII and VIII of Figure 3: A single $Ru^{3+/2+}$ couple was observed with a formal potential near 0.27 V and the ratio of Co to Ru in the coatings matched the ratio of cobalt to cyanophenyl ligands in the porphyrin (Table 1).

The broad, cobalt-centered voltammetric response of the $[CoP(N\text{-}CH_3py)(PhCN)_3]^+$ porphyrin I (Figure 2) was encompassed by the ruthenium-centered response after ruthenation because the formal potentials of the two couples were not far apart. Thus, the voltammetric response shown in Figure 5B is presumed to include the reduction and reoxidation of both the Co and Ru centers in the ruthenated porphyrin on the electrode surface.

The voltammetric responses in Figures 5B and 5C have peak widths at half-height near 190 mV instead of the 90.6 mV expected for a simple, one-electron Nernstian couple[13] (or the 30.2 mV that would be expected if the Ru centers interacted cooperatively to produce a single three-electron couple). Part of the broadening of the voltammetric waves probably results from the reduction and oxidation of the cobalt centers of the porphyrins which accompanies the ruthenium-centered electrochemistry. However, similar wave shapes were obtained from ruthenated coatings prepared from the cobalt-free porphyrin ligands in Figure 1 and in previous studies with redox reactants immobilized on graphite electrode surfaces.[14] The deviations from ideally Nernstian behavior are usually attributed to repulsive interactions among the surface-confined reactants (large enough to produce wave broadening but not to split the response into separate peaks) and/or an array of closely-spaced formal potentials of the redox couples depending upon their microscopic environment on the inhomogeneous graphite surfaces.[15,16] In either case, it is often possible to fit the experimental responses with a modified equation for the current–potential curves which includes an interaction parameter[14,17–19] or with a Gaussian distribution of formal potentials. Details of the fitting procedures that have been employed are available in the literature.[15–20] We employed the procedure that involves the introduction of an interaction parameter into the Nernst expression relating the electrode potential to the fractions of oxidized and reduced reactant present on the electrode surface[14,15,17]

$$f_{III} = [1 + \exp(gF/RT)\,(E - E^f)]^{-1} \qquad (1)$$

where f_{III} is the fraction of the Ru centers in their oxidized (+3) state, E^f is the formal potential of the Ru(III)/Ru(II) couple and g is an interaction parameter. A comparison of the calculated current–potential curve with the response obtained from coatings of porphyrin V of Figure 3 is shown in Figure 6A. The dashed line in Figure 6A is the response that would be obtained from an ideal ($g = 1$) one-electron Nernstian couple. The solid line is the observed cathodic response from which the estimated contributions of the graphite electrode background current and the cobalt(III) reduction current measured before ruthenation have been subtracted. The points were calculated by the procedure described in[14] using eq 1 and a value for the interaction parameter[15] that produced the best match of the observed peak current. The agreement between the experimental and calculated currents at all potentials was reasonable.

(13) Bard, A. J.; Faulkner, L. R. *Electrochemical Methods*; John Wiley and Sons, Inc.: New York, 1980; p 522.
(14) Brown, A. P.; Anson, F. C. *Anal. Chem.* **1977**, *49*, 1589.
(15) Albery, W. J.; Boutelle, M. G.; Colby, P. J.; Hillman, A. R. *J. Electroanal. Chem.* **1982**, *133*, 135.
(16) Jiang, R.; Anson, F. C. *J. Electroanal. Chem.* **1991**, *305*, 171.
(17) Leidner, C. R.; Murray, R. W., *J. Am. Chem. Soc.* **1984**, *106*, 1606.
(18) Laviron, E., *J. Electroanal. Chem.*, **1974**, *52*, 395.
(19) Smith, D. F.; Willman, K.; Kuo, K.; Murray, R. W., *J. Electroanal. Chem.* **1979**, *95*, 217.
(20) Sabatani, E.; Anson, F. C., *J. Phys. Chem.*, **1993**, *97*, 10158.

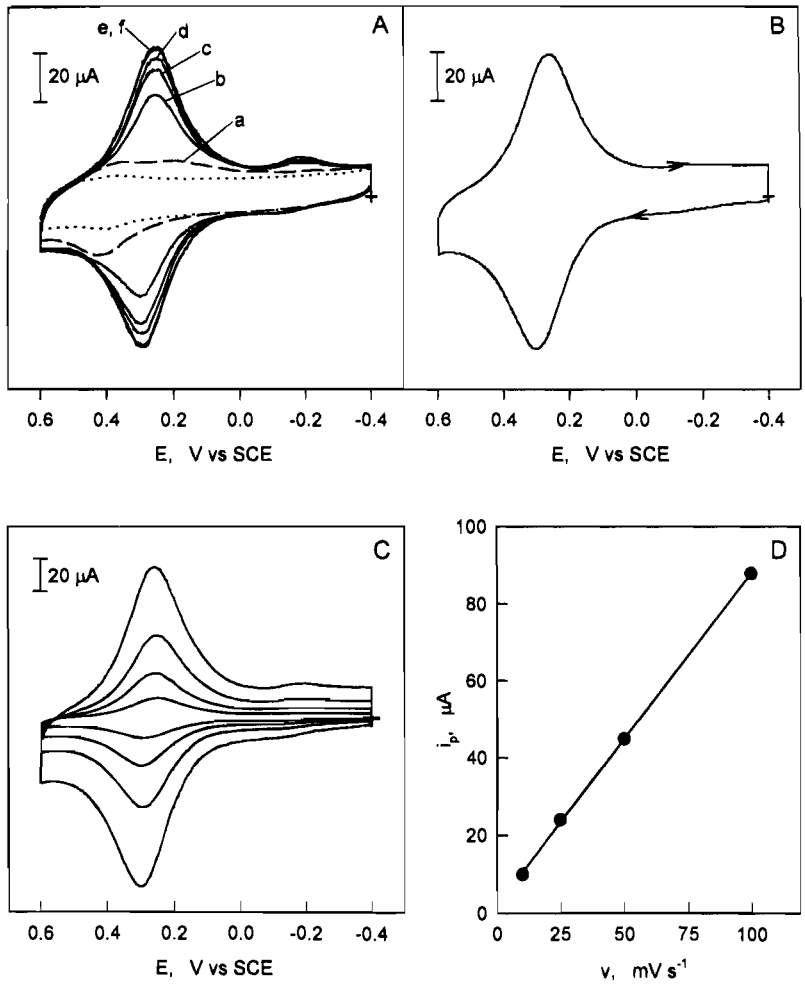

Figure 5. (A) Cyclic voltammetry of an electrode coating containing 2.1×10^{-9} mol cm^{-2} of porphyrin I (Figure 2) plus 1.8×10^{-8} mol cm^{-2} of Nafion sulfonate groups during ruthenation of the nitrile ligand sites. The voltammograms were recorded in 0.5 M NH_4PF_6–0.5 M $HClO_4$ after the electrode had been exposed to a 25 mM solution of $Ru(NH_3)_5OH_2^{2+}$ for (a) 0, (b) 15, (c) 30, (d) 45, (e) 60 and (f) 75 min. The dotted curve was recorded with the uncoated electrode. Scan rate = 50 mV s^{-1}. (B) Repeat of (f) after the uncoordinated $Ru(NH_3)_5OH_2^{2+}$ was removed from the coating by reverse ion-exchange (see text). (C) Repeat of (B) at potential scan rates of 10, 25, 50 and 100 mV s^{-1}. (D) Cathodic peak currents in (C) vs the scan rate.

Table 1. Electrochemical and Electrocatalytic Properties of the Cobalt Porphyrins Examined in This Study[a]

porphyrin[b]	E^f,[c] V vs SCE	$E_{1/2}(O_2)$,[d] V vs SCE	n_{app}[e]	Γ_{Ru}/Γ_{Co}[f]
I		0.19	2.1	
V	0.28	0.30	3.9	2.9
II		0.17	2.0	
VI	0.27	0.25	2.9	1.9
III		0.17	2.0	
VII	0.26	0.22	2.5	1.8
IV		0.18	2.1	
VIII	0.27	0.18	2.0	0.9

[a] Data refer to coatings prepared by mixing 2.1×10^{-9} mol cm^{-2} of each porphyrin with 1.8×10^{-8} mol cm^{-2} of Nafion sulfonate groups and adsorbing the mixture on edge plane pyrolytic graphite electrodes. All measurements were conducted in a supporting electrolyte of 0.5 M NH_4PF_6–0.5 M $HClO_4$. [b] See Figures 2 and 3. [c] Formal potential of the Ru(III)/Ru(II) couple in the ruthenated porphyrin. Estimated from cyclic voltammetric peak potentials recorded at 50 mV s^{-1}. [d] Half-wave potential for the reduction of O_2 in air-saturated solutions at a graphite disk electrode coated with the porphyrin and rotated at 100 rpm. [e] Number of electrons involved in the reduction of O_2 as estimated from the slopes of Koutecky–Levich plots such as those in Figures 8C and 8F. [f] Ratio of ruthenium to cobalt centers in the ruthenated porphyrins.

The procedure used to fit the experimental response in Figure 6A involves the assumption that the cathodic and anodic peak potentials of the adsorbed reactant are the same and equal to the formal potential.[14,15,17] In fact, the cathodic and anodic peak potentials of the adsorbed porphyrin differed by ca. 40 mV which indicated that the heterogeneous rate constant governing the electron transfer to the adsorbed reactant was finite. We therefore employed an alternative fitting procedure in which the possibility of a finite rate of electron transfer was included.[21] The result is shown in Figure 6B. The points were calculated from equation 1 and the Butler-Volmer equation[22] with g = 0.5, E^f = 0.28 V, $k_s°$ = 1.6 s^{-1} and α = 0.5 where $k_s°$ and α are the standard heterogeneous rate constant and transfer coefficient, respectively. As can be seen, the calculated currents remain in good agreement with the observed values. The procedure utilized in Figure 6B was the one selected for the simulation of the responses obtained in the presence of O_2 (*vide infra*).

The behavior shown in Figure 5B and 5C was quite different from that obtained when the uncharged cobalt porphyrin with four pendant cyanophenyl groups, $CoP(PhCN)_4$, was used instead of porphyrin I (Figure 2). The $CoP(PhCN)_4$ molecule was insoluble in the aqueous electrolyte and stable coatings could be obtained by irreversible adsorption on the graphite electrode with or without the addition of Nafion to the coating

(21) Xie, Y.-W., Anson, F. C. To be submitted for publication.
(22) Reference 13, p 103.

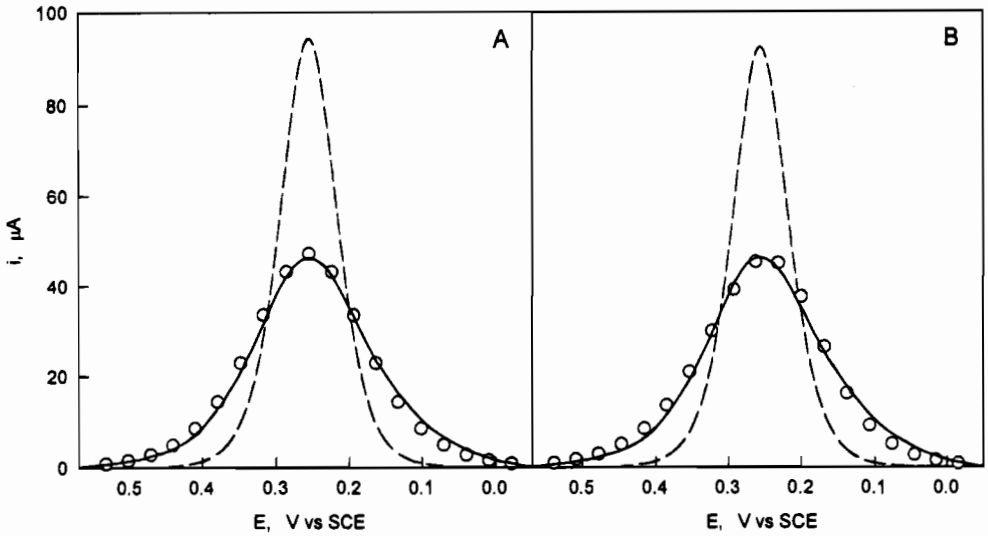

Figure 6. Fitting of the observed voltammetric response from 2.1×10^{-9} mol cm^{-2} of adsorbed ruthenated porphyrin V (Figure 3) with modified current–potential relations. (A) Dashed line: Calculated response for a one-electron Nernstian couple; solid line: observed response. The points were calculated as in ref 14 using equation 1 with $E^f = 0.256$ V and $g = 0.5$. (B) As in (A) except the points were calculated using the Butler-Volmer equation[22] with $E^f = 0.28$ V and $k_s° = 1.6$ s^{-1}.

solution. However, coordination of $Ru(NH_3)_5^{2+}$ centers to the adsorbed coatings proceeded much less extensively. Even after prolonged exposure to solutions of $Ru(NH_3)_5OH_2^{2+}$ the quantities of $Ru(NH_3)_5^{2+}$ which were coordinated to the nitrile ligands corresponded to only a small percentage of the total available sites. This percentage could be increased by diminishing the quantity of $CoP(PhCN)_4$ adsorbed on the electrode but full ruthenation was never obtained. The behavior indicated that most of the nitrile sites in the insoluble, nonsolvated coatings were inaccessible to the $Ru(NH_3)_5OH_2^{2+}$ cations in solution. The introduction of a single, charged, *N*-CH_3py group on the porphyrin ring appeared to enhance the solvation of the coatings sufficiently to facilitate their reactions with $Ru(NH_3)_5OH_2^{2+}$ to produce fully ruthenated cobalt porphyrins. This difference between the behavior of $CoP(PhCN)_4$ and porphyrin I was the reason that the latter porphyrin was utilized for the electrocatalysis experiments.

Catalysis of the Electroreduction of O_2. The four ruthenated porphyrins shown in Figure 3, along with their unruthenated antecedents in Figure 2, were tested as electrocatalysts for the reduction of O_2 by applying them to pyrolytic graphite electrodes along with Nafion to enhance their stabilities on the electrode surface. All of the porphyrins acted as electrocatalysts but both the magnitudes of the reduction currents and the potential where the reduction began increased as the number of $Ru(NH_3)_5^{2+}$ centers coordinated to the nitrile sites was increased. A typical set of cyclic voltammograms is shown in Figure 7. The dashed curves were recorded in the absence of O_2 and the solid curves were obtained in air-saturated solutions. In Figure 7A is shown the reduction of O_2 to H_2O_2 by unruthenated porphyrin IV of Figure 2. After the single nitrile site is ruthenated the response (Figure 7B) contains peaks for the coordinated $Ru(NH_3)_5$ centers in the absence of O_2 but there is no significant change in the position or magnitude of the O_2 reduction peak. The electroreduction of O_2 catalyzed by the unruthenated porphyrin I of Figure 2, shown in Figure 7C, resembles that for the mononitrile in Figure 7A. However, after ruthenation to produce porphyrin V (Figure 3) there is a shift in the peak potential to somewhat more positive values and a large increase in catalytic current which demonstrates that substantially more than two electrons are consumed in the reduction, so that much of the O_2 is reduced to H_2O (Figure 7D).

Control experiments were conducted to confirm that the

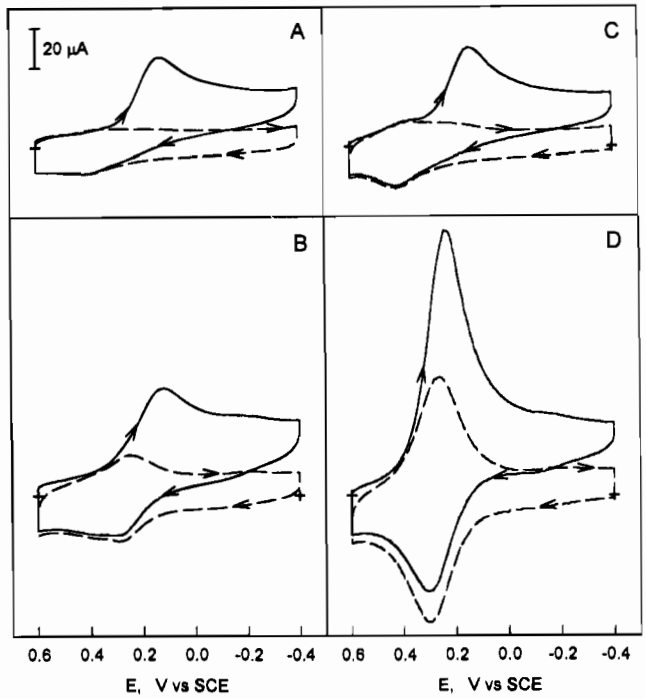

Figure 7. Cyclic voltammogram for the reduction of O_2 at electrodes coated with 2.1×10^{-9} mol cm^{-2} of cobalt porphyrins plus 1.8×10^{-8} mol cm^{-2} of Nafion sulfonate groups. The supporting electrolyte, 0.5 M NH_4PF_6–0.5 M $HClO_4$, was saturated with Ar (dashed lines) or air (solid lines). (A) porphyrin IV (Figure 2); (B) porphyrin VIII (Figure 3); (C) porphyrin I (Figure 2); (D) porphyrin V (Figure 3). Scan rate = 50 mV s^{-1}.

impressive voltammetric response obtained with porphyrin V is the result of the special catalytic properties of this molecule: The $[Ru(NH_3)_5NCPh]^{2+}$ complex does not react with O_2 at an appreciable rate and coatings containing mixtures of this complex with unruthenated porphyrin I exhibited no catalytic activity toward O_2 reduction beyond that of the porphyrin alone. The fully-ruthenated but cobalt-free porphyrin, $[H_2P(PhCNRu(NH_3)_5)_3(N\text{-}CH_3py)]^{7+}$, exhibited no catalytic activity. None of the porphyrins examined in this study acted as electrocatalysts for the reduction of H_2O_2 to H_2O. Therefore, the reduction of O_2 to H_2O achieved by porphyrin V in Figure 7D cannot involve uncoordinated H_2O_2 as an intermediate

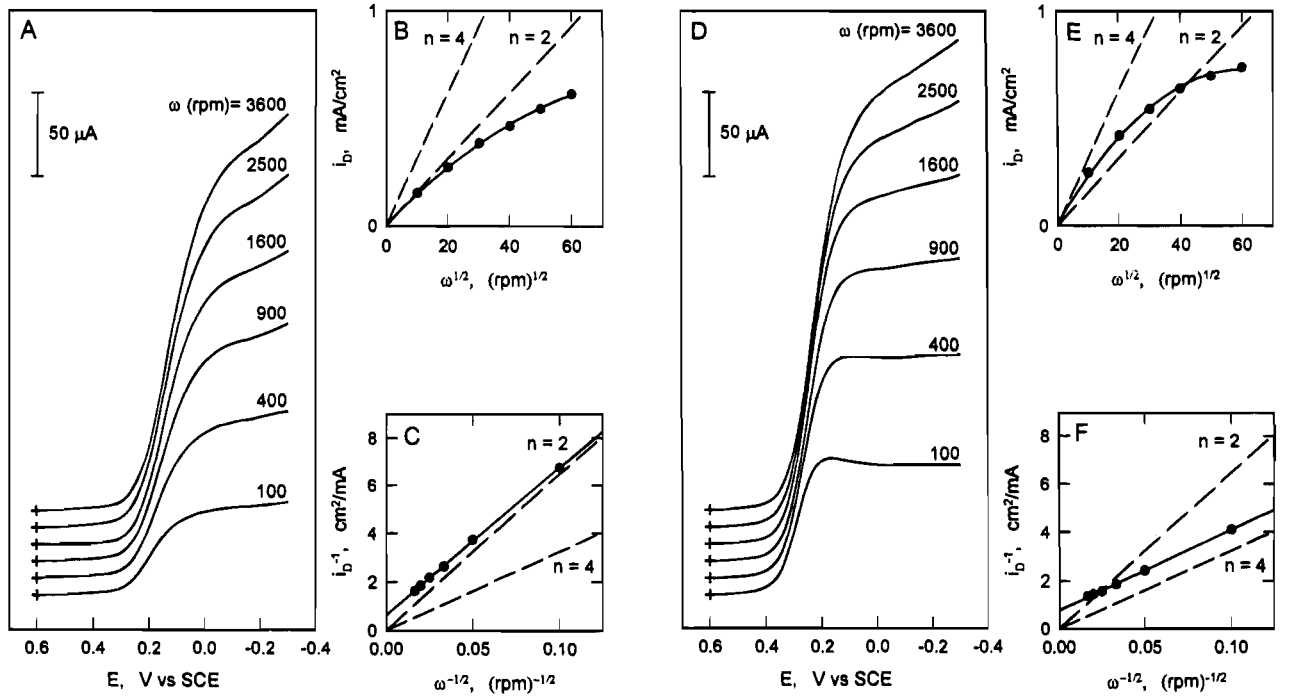

Figure 8. Reduction of O_2 with the electrodes from (A, B, C) Figure 7C and (D, E, F) Figure 7D operated as rotating disk electrodes. (A, D) Current–potential response at the indicated electrode rotation rates; (B, E) Levich plots of the plateau currents vs (rotation rate)$^{1/2}$. (C, F) Koutecky–Levich plots. The dashed lines are the calculated responses for the convection–diffusion-controlled reduction of O_2 by two or four electrons.

because any H_2O_2 formed during the reduction of O_2 would not be further reduced.

The behavior at rotating disk electrodes of coatings of porphyrins I and V is shown in Figure 8. Levich plots[23] of the plateau currents vs the electrode (rotation rate)$^{1/2}$ are curved (Figures 8B and 8E), as is typical for the electroreduction of O_2 catalyzed by adsorbed cobalt and iron porphyrins,[1-3,24] but the slopes of the linear Koutecky–Levich plots[25] (Figures 8C and 8F) show that the reduction is converted from a two- to a four-electron process after the coordination of three $Ru(NH_3)_5^{2+}$ centers to the porphyrin. Repetition of the experiments of Figure 8 with porphyrin IV or VIII with only a single pendant cyanophenyl group produced results which were little changed by the ruthenation step: The two-electron reduction of O_2 to H_2O_2 persisted and the ruthenation actually caused the plateau currents to decrease somewhat. This decrease is probably the result of the diminished catalytic reactivity of the cationic ruthenated porphyrin complex when it is incorporated by the Nafion in the coating during the 30–60 min required for the ruthenation to reach completion.[1]

To compare more quantitatively the stoichiometry of the reductions of O_2 as catalyzed by the non- or triply-ruthenated porphyrin, I, a rotating graphite disk–platinum ring electrode[26] was employed. The results, shown in Figure 9, confirm that the triple ruthenation produces a catalyst that causes most of the O_2 to be reduced by four-electrons. The ratio of the ring to disk currents in Figure 9B corresponds to the reduction of 77% of the O_2 molecules to H_2O while the current ratio in Figure 9A shows all of the O_2 is reduced to H_2O_2 at electrodes coated with unruthenated porphyrin I. The 77% four-electron reduction in Figure 9B differs from the results obtained in Figure 8. The slope of the Koutecky–Levich plot in Figure 8F corresponds to the reduction of 95% of the O_2 molecules to H_2O. The difference between the stoichiometries in the two experiments is the result of the different electrodes that were employed. For reasons that are unclear, porphyrins adsorbed on the surface of the commercial graphite disk–platinum ring electrode were more difficult to ruthenate fully than was true when the porphyrins were adsorbed on our homemade pyrolytic graphite disk electrodes. With the ring–disk electrode used to obtain Figure 9B only 2.6 $Ru(NH_3)_5^{2+}$ centers per cobalt porphyrin could be introduced on the disk surface and the disk potential in Figure 9B where the production of H_2O_2 is first detected at the ring electrode corresponds to the potentials where the incompletely ruthenated porphyrins were observed to catalyze the reduction of O_2 to H_2O_2 in Figure 9A. The larger quantities of H_2O_2 produced with the commercial than with the homemade electrode is therefore attributed to incomplete ruthenation.

The close correlation between the reduction of the $Ru(NH_3)_5^{3+}$ centers coordinated to the nitrile ligands of the porphyrin and the rate of the catalyzed reduction of O_2 is demonstrated in Figure 10. The fraction of the $Ru(NH_3)_5^{3+}$ groups that were reduced to $Ru(NH_3)_5^{2+}$ groups at each potential was evaluated from voltammograms such as the one in Figure 5B by measuring the areas under the cathodic peak between 0.6 V and each potential of interest. The results are shown by the dashed curves in Figure 10. The solid curves in Figure 10 are the current–potential curves for the reduction of O_2 at a catalyst-coated rotating graphite disk electrode after subtraction of the contribution from the reduction of the adsorbed catalyst that is shown by the dotted curves at the bottom of the figure. It is evident that the activity of the adsorbed catalyst toward the reduction of O_2 increases continuously as the ruthenium centers are reduced to Ru(II). At low electrode rotation rates the O_2 reduction current reaches its plateau value somewhat before all of the Ru(III) centers are reduced because the plateau current is essentially equal to the diffusion–convection limited Levich current[23] for the four-electron reduction of O_2. At higher

(23) Levich, V. G., *Physicochemical Hydrodynamics*; Prentice Hall: Englewood Cliffs, NJ, 1962.
(24) Shigehara, K.; Anson, F. C. *J. Phys. Chem.* **1982**, *86*, 2776.
(25) (a) Koutecky, J., Levich, V. G. *Zh. Fiz. Khim.* **1956**, *32*, 1565. (b) Oyama, N.; Anson, F. C. *Anal. Chem.* **1980**, *52*, 1192.
(26) Albery, W. J.; Hitchman, M. H. *Ring–Disk Electrodes*; Oxford University Press: Oxford, U.K., 1965.

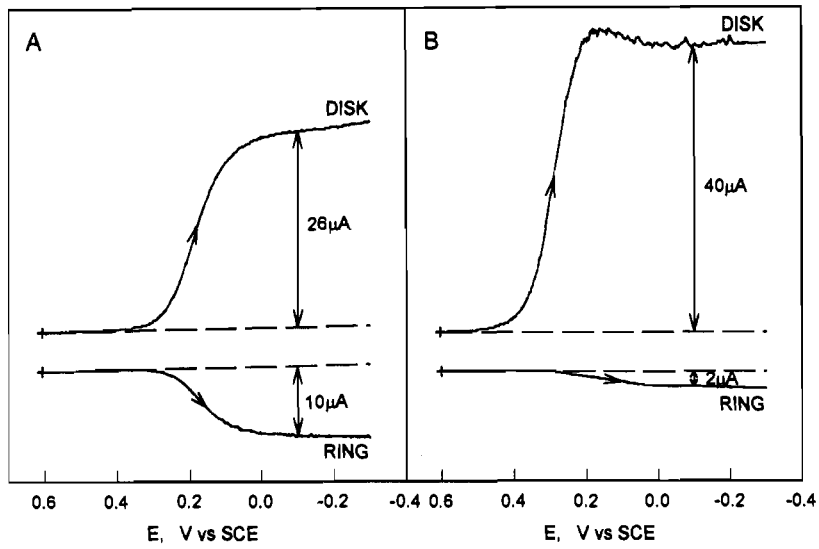

Figure 9. Reduction of O_2 at a rotating platinum ring-pyrolytic graphite disk electrode. The disk was coated with 2.1×10^{-9} mol cm^{-2} of (A) porphyrin I (Figure 2) or (B) porphyrin V (Figure 3) plus 1.8×10^{-8} mol cm^{-2} of Nafion sulfonate groups. The potential of the platinum ring electrode was set at 1.0 V. Supporting electrolyte: 0.5 M NH_4PF_6–0.5 M $HClO_4$ saturated with air. Rotation rate = 100 rpm. Scan rate = 5 mV s^{-1}.

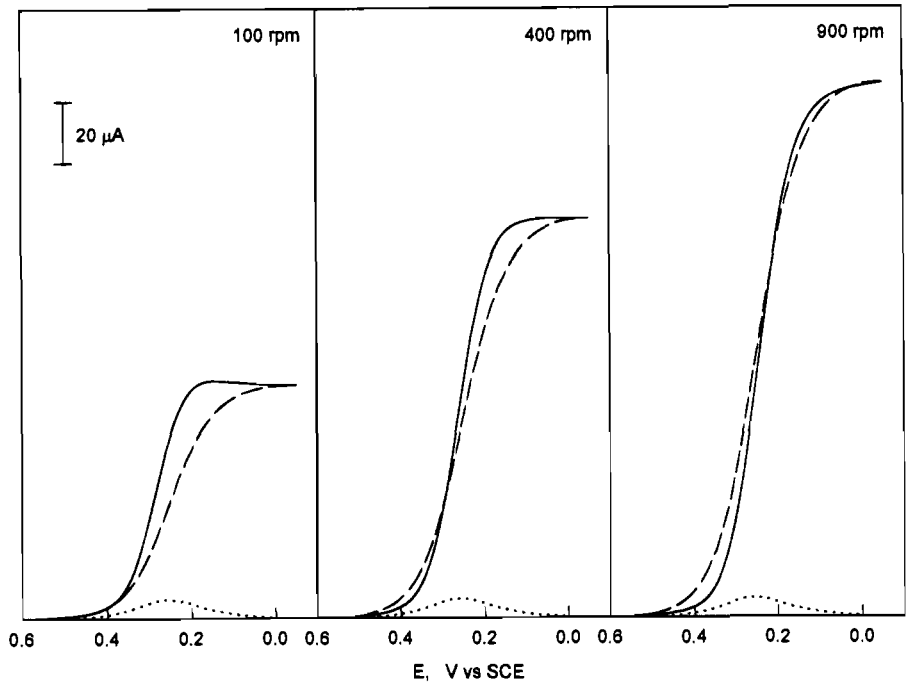

Figure 10. Solid curves: Current–potential curves for the reduction of O_2 at rotating disk electrodes coated with 2.1×10^{-9} mol cm^{-2} of porphyrin V (Figure 3) plus 1.8×10^{-8} mol cm^{-2} of Nafion sulfonate groups. The response from the adsorbed porphyrin in the absence of O_2, shown by the dotted curves at the bottom of the Figure, was subtracted from the responses obtained in the presence of O_2 before the solid curves were plotted. The dashed curves show the fraction of the $[Ru(NH_3)_5(NCPh)]^{3+}$ centers of the adsorbed porphyrin that were reduced to $[Ru(NH_3)_5(NCPh)]^{2+}$ at each potential. For each rotation rate this fraction varies between 0 at 0.6 V and 1.0 at −0.05 V.

rotation rates the plateau currents are less than the corresponding Levich currents and the limiting plateaux are not reached until essentially all of the ruthenium centers are converted to $Ru(NH_3)_5^{2+}$. This is the behavior that would be expected if the role of the $Ru(NH_3)_5^{3+/2+}$ centers were simply to cycle between oxidation states while effecting rapid intramolecular electron transfer to O_2 molecules coordinated to the cobalt(II) centers of the adsorbed porphyrin. However, as described in the next section, we believe the actual catalytic mechanism is more involved.

The catalytic properties of the various substituted porphyrins that were examined in this study are summarized in Table 1. In terms of both operating potential and four-electron reduction stoichiometry the best performance was obtained with the triply-ruthenated porphyrin. Its properties are also quantitatively superior to those of the tetrapyridyl porphyrins described in our previous studies.[1-3] Additional advantages of cyanophenyl over pyridine as ligands for the coordination of $Ru(NH_3)_5^{2+}$ centers to the porphyrin ring are the much greater rate of the coordination reaction and the greater chemical stability of ruthenium(II) nitriles compared to the corresponding pyridine complexes.[27]

Mechanistic Considerations. The reason that coordination of $Ru(NH_3)_5^{2+}$ to unsaturated ligand sites on the periphery of cobalt porphyrin rings converts two-electron to four-electron electrocatalysts for the reduction of O_2 involves more than simple intramolecular electron transfer.[3,4] The extent of d-π

(27) Allen, R. J.; Ford, P. C., *Inorg. Chem.* **1972**, *11*, 679.

back-bonding by the $Ru(NH_3)_5^{2+}$ centers to the unsaturated ligands, with accompanying electronic perturbation of the porphyrin-cobalt(II) and cobalt(II)$-O_2$ bonding, has been argued to be more important than the reducing strength of the coordinated $Ru(NH_3)_5^{2+}$ groups.[2,3] For example, coordination of more weakly back-bonding $Ru(edta)^{2-}$ groups instead of $Ru(NH_3)_5^{2+}$ groups to $CoP(py)_4$ does not produce a four-electron reduction catalyst despite the much more negative formal potential of the $Ru(edta)py^{-/2-}$ couple.[3] The formal potentials of the $[Ru(NH_3)_5L]^{3+/2+}$ couples in solution are -0.18, 0.06 and 0.28 V for L = H_2O, py and PhCN, respectively. The larger positive shift in formal potential for the benzonitrile ligand reflects the greater π-acidity of this ligand compared to pyridine. Another indication of the extensive back-bonding that is involved in the coordination of $Ru(NH_3)_5^{2+}$ to benzonitrile is the unusual decrease (instead of increase) in the infrared stretching frequency of the CN group in the complex.[28] The catalytic importance of the strong π-back-bonding is believed to reside in a resulting beneficial enhancement of the electronic interactions between the Co(II) center of the porphyrin and the O_2 molecule that is coordinated to it in the crucial intermediate of the catalytic cycle. Whatever the chemical factors that are responsible for the activation of O_2 toward electroreduction when it is coordinated to adsorbed cobalt porphyrins, they are apparently intensified when π-back bonding $Ru(NH_3)_5^{2+}$ groups are added to the girdling porphyrin ring. The close correlation between the catalytic rate and the fraction of the coordinated $Ru(NH_3)_5^{3+}$ centers that are reduced to $Ru(NH_3)_5^{2+}$, as shown in Figure 10, is understandable on this basis because only the reduced ruthenium centers participate in the back-bonding.[28] The greater activity of the fully, than of the partially ruthenated porphyrin could then be ascribed to the additional back-bonding interactions that are introduced as more $Ru(NH_3)_5^{2+}$ groups are coordinated to the porphyrin. If this interpretation of the experimental observation is correct, it suggests a number of other candidates for the type of co-catalyst role played by the $Ru(NH_3)_5^{2+}$ centers in the present study. Experiments to test other potential back-bonding co-catalysts are underway.

A possible mechanism for the catalytic cycle is given in Scheme 1 where $CoPL(Ru^{3+})_3$ = $[CoP(N\text{-}CH_3py)(PhCNRu^{III}(NH_3)_5)_3]^{10+}$ and $CoPL(Ru^{2+})_3$ = $[CoP(N\text{-}CH_3py)(PhCNRu^{II}(NH_3)_5)_3]^{7+}$ and it is understood that all of the cobalt porphyrins are confined to the surface of the electrode. A noteworthy feature of Scheme 1 is the fact that the oxidation states of both the Co and $Ru(NH_3)_5$ centers do not change during the catalytic cycle (reactions 4 to 6) because all four of the electrons required to reduce the O_2 molecule to $2H_2O$ are supplied by the electrode itself. The potential, E_2, where the Co(III) form of the ruthenated porphyrin is reduced to Co(II) is close to E_3, the potential where the $Ru(NH_3)_5(NCPh)^{3+}$ centers are reduced to $Ru(NH_3)_5(NCPh)^{2+}$. E_3 is also the potential where the catalyzed reduction of O_2 occurs. The coincidence of the two reductions indicates that the formal potential of reaction 5 in Scheme 1, E_5, is probably more positive than E_3.

Reactions not included in Scheme 1 are the formation and subsequent reduction of the O_2 adduct of $Co^{II}PL(Ru^{3+})_3$. Although this adduct may well be formed, the reduction of the coordinated O_2 is expected to occur at more negative potentials than those where $Co^{II}PL(Ru^{3+})_3O_2$ is reduced to $Co^{II}PL(Ru^{2+})_3O_2$. The catalytic current was therefore assumed to be dominated by the reduction of the latter adduct.

Digital Simulation. It proved possible to simulate the cyclic voltammetric response to be expected from the mechanism of Scheme 1 by appropriate modification of the procedures of Andrieux and Savéant[29] and Aoki et al.[30] The procedure involves the addition of the calculated kinetic current arising from half-reactions 5 and 6 to the current originating in the catalyst itself (half-reaction 3). The modified calculational procedures employed are described elsewhere.[21] In Figure 11 simulated cyclic voltammograms are compared with those obtained experimentally. To facilitate the comparison, the background and double layer charging contributions to the experimental voltammograms were subtracted before the points

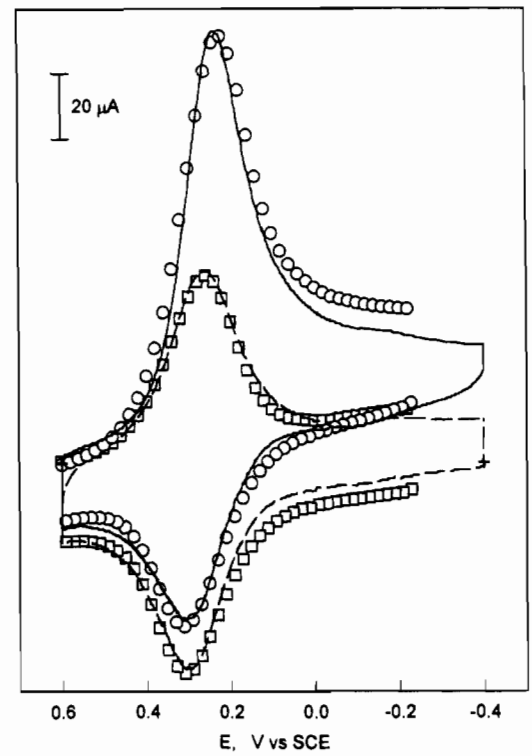

Figure 11. Comparison of experimental (solid curves) and simulated (plotted points) cyclic voltammograms for the reduction of O_2 at a graphite electrode coated with 2.1×10^{-9} mol cm^{-2} of porphyrin V. (□) Response in the absence of O_2. The simulated voltammogram was calculated as in Figure 6B. (○) Response in air-saturated solution. The simulated voltammogram was calculated on the basis of Scheme 1 using $k_f = 8 \times 10^3$ M^{-1} s^{-1}, $E_5 = 0.43$ V and $K(k_s°)_5 = 1.9 \times 10^2$ M^{-1} s^{-1} with the concentration and diffusion coefficient of O_2 being 0.28 mM and 1.7×10^{-5} cm^2 s^{-1}, respectively. The scan rate was 50 mV s^{-1}. Other conditions as in Figure 7.

Scheme 1

$$Co^{III}PL(Ru^{3+})_3 + e \rightleftharpoons Co^{II}PL(Ru^{3+})_3 \quad E_2 \qquad (2)$$

$$Co^{II}PL(Ru^{3+})_3 + 3e \overset{(k_s°)_3}{\rightleftharpoons} Co^{II}PL(Ru^{2+})_3 \quad E_3 \qquad (3)$$

$$Co^{II}PL(Ru^{2+})_3 + O_2\ e \underset{k_b}{\overset{k_f}{\rightleftharpoons}} Co^{II}PL(Ru^{2+})_3O_2 \quad K = k_f/k_b \qquad (4)$$

$$Co^{II}PL(Ru^{2+})_3O_2 + e \overset{(k_s°)_5}{\rightleftharpoons} Co^{II}PL(Ru^{2+})_3(O_2^-) \quad E_5 \qquad (5)$$

$$Co^{II}PL(Ru^{2+})_3(O_2^-) + 3e + 4H^+ \xrightarrow{\text{fast}} Co^{II}PL(Ru^{2+})_3 + 2H_2O \qquad (6)$$

(28) Clarke, R. E.; Ford, P. C., *Inorg. Chem.* **1970**, *9*, 227.

(29) Andrieux, C.-P.; Savéant, J.-M. *J. Electroanal. Chem.* **1978**, *93*, 163.

(30) Aoki, K.; Tokuda, K.; Matsuda, H. *J. Electroanal. Chem.* **1986**, *198*, 69.

shown in the figure were plotted. The simulated voltammogram for the catalyst in the absence of O_2 was calculated by the procedure described above in connection with Figure 6B.

The contribution to the voltammetric response from the catalyst was obtained as in Figure 6B. To simulate the contribution to the response to be expected from the catalyzed reduction of O_2 according to Scheme 1 it was necessary to have values of k_f, E_5 and $K(k_s^\circ)_5$. The parameters employed in the simulation were chosen by optimizing the agreement between the simulated and experimental voltammograms.[21] The values of k_f, E_5 and $K(k_s^\circ)_5$ utilized to obtain the simulated voltammogram in Figure 11 were 8×10^3 M^{-1} s^{-1}, 0.43 V and 1.9×10^2 M^{-1} s^{-1}, respectively. The value of k_f used in the simulation is close to the value (6×10^3 M^{-1} s^{-1}) obtained from the intercept of the Koutecky–Levich plot in Figure 8F. This reasonable agreement between the rate constants evaluated by two independent routes provided support for the simulation procedure employed. The experimental and simulated voltammograms in Figure 11 are closely coincident except for the region well beyond the cathodic peaks where corrections for background currents were difficult to make with precision. The good fit of the experimental response in the region of the peaks supports the identification of reaction 4 as the step that limits the catalytic reduction current and the assumptions underlying Scheme 1, i.e., that the catalytic cycle does not involve the cycling of the $Ru(NH_3)_5(NCPh)$ centers between their +3 and +2 oxidation states.

Note that a step involving the direct oxidation of the $Ru(NH_3)_5(NCPh)^{2+}$ centers by O_2 was not included in Scheme 1. Simulations were carried out for an alternative mechanism in which reactions 4–6 of Scheme 1 were replaced by a reaction in which the reduction of O_2 resulted from its reaction with four $[Ru(NH_3)_5NCPh]^{2+}$ groups coordinated to the adsorbed cobalt porphyrin. When the rate constant for such a reaction was identified with that evaluated from the intercepts of Koutecky–Levich plots like that in Figure 8F, the calculated peak potential of the catalytic reduction was shifted to values more positive than the observed value near E_3. If smaller values of the rate constant were used in order to match the peak potentials, the calculated peak currents fell well below the observed values. Thus, the catalytic mechanism of Scheme 1 is compatible with the observed voltammetry while one in which the $Ru(NH_3)_5(NCPh)$ centers cycle between their oxidation states is not.

Conclusions

The triruthenated cobalt porphyrin (V in Figure 3 and Table 1) catalyzes the electroreduction of O_2 by four electrons at more positive potentials than any of the related porphyrins examined in this and our previous reports.[1-3] Comparisons of the behavior of the porphyrins listed in Table 1 suggested that the catalytic mechanism involves π back-bonding of the $Ru(NH_3)_5^{2+}$ centers coordinated to the cyanophenyl substituents on the porphyrin ring rather than simple intramolecuar electron transfer from the $Ru(NH_3)_5^{2+}$ centers to O_2 molecules coordinated to the cobalt(II) center of the porphyrin. Numerical simulations of the voltammetric responses anticipated for the latter mechanism support this conclusion. It would be desirable to compare the behavior observed with the ruthenated porphyrins attached to electrode surfaces with that obtained with the same molecules in homogeneous solution. Preparing solutions of the ruthenated porphyrins in aqueous acid has proved to be difficult, but preliminary experiments with what is believed to be porphyrin VIII (Figure 3) in solution indicate that it does not catalyze significantly the slow homogeneous reaction between O_2 and $Ru(NH_3)_5NCPh^{2+}$. If this result is confirmed in continuing studies it will add support for the catalytic mechanism depicted in Scheme 1.

Experimental Section

Materials. All chemicals were reagent grade unless otherwise specified. Laboratory water was purified using a Milli-Q Plus water system (Millipore Co.). Tetrabutylammonium hexafluorophosphate ((TBA)PF_6; Southwestern Analytical Chemicals Inc.) was recrystallized from ethanol-water and dried under vacuum. Nafion (equiv wt 1100) was obtained as a 5 wt % solution (Aldrich). It was diluted with methanol to prepare the 0.5 wt % stock solution that was used to prepare electrode coatings. The preparation of solutions of $Ru(NH_3)_5OH_2^{2+}$ was previously described.[2] $[Ru(NH_3)_5NCPh](ClO_4)_2$ was prepared by the method of Clarke and Ford.[28] The porphyrins were synthesized and purified according to methods previously described[3] with appropriate modifications. To obtain the desired combinations of pyridyl and cyanophenyl groups as substituents on the porphyrin rings, the porphyrins were prepared with three different molar ratios of 4-cyanobenzaldehyde to 4-pyridinecarboxaldehyde: Freshly distilled pyrrole (1.35 g, 20 mmol), 4-cyanobenzaldehyde (Aldrich, 99%) (i: 1.97 g, 15 mmol; ii: 1.31 g, 10 mmol; iii: 0.66 g, 5 mmol), and freshly distilled 4-pyridinecarboxaldehyde (i: 0.54 g, 5 mmol; ii: 1.07 g, 10 mmol; iii: 1.61 g, 15 mmol) were added to 50 mL of 99% propionic acid, and the mixture was stirred open to the air at 145 °C for 1 h. The reaction mixture was cooled in an ice–water bath for 15 min and added to 200 mL of acetone. Then 50 mL of 29% aqueous ammonia were slowly added to the cooled (ice–water bath) mixture. After cooling overnight to −20 °C, the precipitate which had formed was collected by suction filtration on a Buchner funnel (4–5.5-μm fritted glass disk), washed with acetone and air-dried to give 0.59 g (i), 0.62 g (ii), and 0.64 g (iii), respectively, of violet powders. The products were inspected by silica gel thin-layer chromatography and found to be a mixture of six components, as would be expected if all possible cyanophenyl- and pyridyl-substituted porphyrins were present. The R_f values of the components in 98% chloroform/2% ethanol were 0.54, 0.26, 0.17, 0.09, 0.06, and 0.03. By comparison with the R_f values for the phenylpyridyl porphyrins[3] it was possible to assign the R_f values respectively to 5,10,15,20-tetrakis(4-cyanophenyl)porphyrin ($H_2P(PhCN)_4$), 5,10,15-tris(4-cyanophenyl)-20-(4-pyridyl)porphyrin ($H_2P(PhCN)_3(py)$), 5,15-bis(4-cyanophenyl)-10,20-bis(4-pyridyl)porphyrin (*trans*-$H_2P(PhCN)_2(py)_2$), 5,10-bis(4-cyanophenyl)-15,20-bis(4-pyridyl)-porphyrin (*cis*-$H_2P(PhCN)_2(py)_2$), 5-(4-cyanophenyl)-10,15,20-tris(4-pyridyl)porphyrin ($H_2P(PhCN)(py)_3$) and 5,10,15,20-tetrakis(4-pyridyl)-porphyrin ($H_2P(py)_4$). The porphyrins were separated by gravity column chromatography with silica gel (Baker for flash chromatography; the column was packed with 99% chloroform/1% ethanol) and a chloroform/ethanol solvent system consisting of 98% chloroform/2% ethanol (elution of $H_2P(PhCN)_4$, $H_2P(PhCN)_3(py)$, *trans*-$H_2P(PhCN)_2(py)_2$, and *cis*-$H_2P(PhCN)_2(py)_2$), 97% chloroform/3% ethanol (elution of $H_2P(PhCN)(py)_3$), and 95% chloroform/5% ethanol (elution of $H_2P(py)_4$). The mixture of separated products in the order of decreasing R_f values given above consisted of i: 59%, 36%, 1%, 4%, trace, and trace; ii: 14%, 34%, 9%, 20%, 19%, and 4%, and iii: 1%, 7%, 7%, 16%, 40%, and 29%. The porphyrins were dried under vacuum (5×10^{-3} Torr) at room temperature for 15 h. Except for the previously prepared $H_2P(PhCN)_4$ and $H_2P(py)_4$ porphyrins, the identities of the molecules $H_2P(PhCN)_3(py)$, *trans*-$H_2P(PhCN)_2(py)_2$, *cis*-$H_2P(PhCN)_2(py)_2$, and $H_2P(PhCN)(py)_3$ were confirmed by elemental analysis, visible spectroscopy, infrared spectroscopy and ^1H NMR spectroscopy.

$H_2P(PhCN)_3(py)$. Anal. Calcd for $C_{46}H_{26}N_8 \cdot 1/2\ H_2O$: C, 78.95; N, 16.01; H, 3.89; Found: C, 78.94; N, 15.67; H, 4.10. Visible spectrum [λ, nm, in $CHCl_3$ (ϵ x 10^{-4} cm^{-1} M^{-1})]: 418 (43.28), 514 (2.04), 548 (0.74), 590 (0.62), 646 (0.27). Infrared spectrum [cm^{-1}]: 3318, 2229, 1604, 1595, 1560, 1501, 1475, 1400, 1351, 1225, 1188, 1155, 1107, 1022, 994, 981, 967, 880, 856, 800, 733, 657. ^1H NMR [500 MHz, $CDCl_3$]: δ 9.06 (2H, d, 5.7 Hz, pyridyl 2,6), 8.86 (2H, d, 4.6 Hz, pyrrole 2,18), 8.81 (2H, d, pyrrole 3,17) superimposed by 8.80 (4H, s, pyrrole 7,8,12,13), 8.33 (6H, d, 8.1 Hz, *o*-(cyanophenyl)), 8.15 (2H, d, 5.6 Hz, pyridyl 3,5), 8.10 (6H, d, 7.9 Hz, *m*-(cyanophenyl)), 1.57 (s, H_2O), −2.88 (2H, s, internal pyrrole).

***cis*-$H_2P(PhCN)_2(py)_2$.** Anal. Calcd for $C_{44}H_{26}N_8 \cdot 1/2\ H_2O$: C, 78.21; N, 16.58; H, 4.03; Found: C, 78.21; N, 16.29; H, 4.22. Visible spectrum [λ, nm, in $CHCl_3$ (ϵ x 10^{-4} cm^{-1} M^{-1})]: 418 (41.98), 514 (1.93), 548 (0.63), 590 (0.53), 646 (0.33). Infrared spectrum [cm^{-1}]: 3318, 2229, 1594, 1559, 1502, 1474, 1402, 1351, 1224, 1216, 1188, 1156, 1107, 1070, 1022, 996, 980, 969, 880, 853, 800, 731, 666, 649. ^1H NMR [500 MHz, $CDCl_3$]: δ 9.06 (4H, d, 5.2 Hz, pyridyl 2,6), 8.87 (2H, s, pyrrole 17,18) superimposed by 8.86 (2H, d, pyrrole 2,13), 8.81 (2H, d, pyrrole 3,12) superimposed by 8.80 (2H, s, pyrrole 7,8), 8.33 (4H, d, 8.3 Hz, *o*-(cyanophenyl)), 8.15 (4H, d, 5.8 Hz, pyridyl 3,5), 8.09 (4H, d, 7.9 Hz, *m*-(cyanophenyl)), 1.66 (s, H_2O), −2.88 (2H, s, internal pyrrole). ^1H NMR [500 MHz, Me_2SO-d_6]: δ 9.06 (4H, d, 5.2 Hz, pyridyl 2,6), 8.91 (4H, s (broad), pyrrole 2,13,17,18), 8.87 (4H, s (broad), pyrrole 3,7,8,12), 8.44 (4H, d, 7.7 Hz) and 8.31 (4H, d, 7.8 Hz), (*o*- and *m*-(cyanophenyl)), 8.27 (4H, d, 5.3 Hz, pyridyl 3,5), −3.02 (2H, s, internal pyrrole).

***trans*-$H_2P(PhCN)_2(py)_2$.** Anal. Calcd for $C_{44}H_{26}N_8 \cdot 1\ 1/2\ H_2O$: C, 76.18; N, 16.15; H, 4.21; Found: C, 76.12; N, 16.01; H, 3.97. Visible spectrum [λ, nm, in $CHCl_3$ (ϵ x 10^{-4} cm^{-1} M^{-1})]: 418 (43.56), 514 (2.17), 548 (0.73), 588 (0.69), 644 (0.26). Infrared spectrum [cm^{-1}]: 3320, 2229, 1593, 1559, 1500, 1473, 1402, 1351, 1225, 1216, 1188, 1156, 1107, 1070, 1022, 998, 981, 968, 882, 856, 801, 729, 659, 637. ^1H NMR [500 MHz, $CDCl_3$]: δ 9.07 (4H, d, 4.7 Hz, pyridyl 2,6), 8.86 (4H, d, 4.2 Hz, pyrrole 2,8,12,18), 8.80 (4H, d, 4.7 Hz, pyrrole 3,7,13,17), 8.31 (4H, d, 8.0 Hz, *o*-(cyanophenyl)), 8.15 (4H, d, 6.0 Hz, pyridyl 3,5), 8.10 (4H, d, 7.8 Hz, *m*-(cyanophenyl)), 1.53 (s, H_2O), −2.89 (2H, s, internal pyrrole).

$H_2P(PhCN)(py)_3$. Anal. Calcd for $C_{42}H_{26}N_8 \cdot H_2O$: C, 76.35; N, 16.96; H, 4.27; Found: C, 76.33; N, 16.61; H, 4.24. Visible spectrum [λ, nm, in $CHCl_3$ (ϵ x 10^{-4} cm^{-1} M^{-1})]: 416 (46.32), 512 (2.28), 548 (0.70), 588 (0.70), 644 (0.23). Infrared spectrum [cm^{-1}]: 3317, 2229, 1593, 1560, 1501, 1473, 1405, 1351, 1225, 1215, 1189, 1156, 1070, 1022, 999, 979, 970, 882, 850, 799, 728, 660, 642. ^1H NMR [500 MHz, $CDCl_3$]: δ 9.06 (6H, d, 5.3 Hz, pyridyl 2,6), 8.87 (4H, s, pyrrole 12,13,17,18), superimposed by 8.86 (2H, d, pyrrole 2,8), 8.81 (2H, d, 4.7 Hz, pyrrole 3,7), 8.33 (2H, d, 8.1 Hz, *o*-(cyanophenyl)), 8.16 (6H, d, 5.6 Hz, pyridyl 3,5), 8.09 (2H, d, 8.3 Hz, *m*-(cyanophenyl)), 1.72 (s, H_2O), −2.89 (2H, s, internal pyrrole).

$H_2P(PhCN)_4$. Visible spectrum [λ, nm, in $CHCl_3$ (ϵ x 10^{-4} cm^{-1} M^{-1})]: 420 (44.86), 514 (2.27), 550 (0.94), 590 (0.77), 648 (0.29). Infrared spectrum [cm^{-1}]: 3319, 2230, 1606, 1562, 1501, 1477, 1400, 1351, 1225, 1188, 1155, 1107, 1022, 994, 981, 967, 880, 856, 800, 734. ^1H NMR [500 MHz, $CDCl_3$]: δ 8.80 (8H, s, pyrrole), 8.33 (8H, d, 8.3 Hz, *o*-(cyanophenyl)), 8.10 (8H, d, 6.9 Hz, *m*-(cyanophenyl)), 1.53 (s, H_2O), −2.87 (2H, s, internal pyrrole).

$H_2P(py)_4$. Visible spectrum [λ, nm, in $CHCl_3$ (ϵ x 10^{-4} cm^{-1} M^{-1})]: 416 (41.10), 512 (2.04), 546 (0.55), 588 (0.62), 642 (0.19). Infrared spectrum [cm^{-1}]: 3316, 1594, 1558, 1543, 1472, 1405, 1352, 1227, 1215, 1190, 1157, 1070, 1002, 972, 883, 846, 800, 726, 660, 640. ^1H NMR [500 MHz, $CDCl_3$]: δ 9.07 (8H, d, 5.6 Hz, pyridyl 2,6), 8.88 (8H, s, pyrrole), 8.17 (8H, d, 5.3 Hz, pyridyl 3,5), 1.55 (s, H_2O), −2.90 (2H, s, internal pyrrole).

***N*-Methylation of Pyridyl Porphyrins.** *N*-methylation of the porphyrins containing 4-pyridyl substituents was carried out in DMF as solvent. The use of $CHCl_3$, as in a previous *N*-methylation procedure,[31] caused the porphyrins to precipitate and led to incomplete methylation. $[H_2P(PhCN)_3(N\text{-}CH_3py)]\ PF_6$, *cis*- and *trans*-$[H_2P(PhCN)_2(N\text{-}CH_3py)_2]\ (PF_6)_2$ and $[H_2P(PhCN)(N\text{-}CH_3py)_3]\ (PF_6)_3$ were prepared as follows: To 50 mg of porphyrin dissolved in 20 mL of DMF were added 50 mol equiv of freshly distilled (over $NaHCO_3$ under high vacuum) methyl-*p*-toluenesulfonate. The mixture was stirred under argon at 80 °C for 20 h. The reaction solution was added to 50 mL of ether in an ice−water bath. The precipitate was collected by suction filtration on a Buchner funnel (4−5.5−μm fritted glass disk) and washed with ether. The product was dissolved in 10 mL of DMF and added dropwise to a stirred solution of 2.6 g of NH_4PF_6 (Aldrich, 99.99%) in 20 mL of H_2O in an ice−water bath. After centrifugation, the residue was suspended in 20 mL of H_2O, collected by suction filtration on a Buchner funnel, washed with H_2O and dried under vacuum at 100 °C for 12 h. Yield: 83% to 93%. The identities of the products were confirmed by elemental analysis, visible spectroscopy, infrared spectroscopy and ^1H NMR spectroscopy.

$[H_2P(PhCN)_3(N\text{-}CH_3py)]PF_6$. Anal. Calcd for $C_{47}H_{29}F_6N_8P \cdot 1/2\ H_2O$: C, 65.66; N, 13.03; H, 3.52; Found: C, 66.02; N, 12.82; H, 3.53. Visible spectrum [λ, nm, in acetone (rel intens)]: 418 (1.0), 514 (0.065), 550 (0.028), 590 (0.023), 644 (0.0098). Infrared spectrum [cm^{-1}]: 2229, 1639, 1605, 1560, 1515, 1501, 1476, 1400, 1352, 1274, 1220, 1185, 1157, 1109, 1061, 1022, 995, 981, 967, 866, 847, 802, 733, 716, 666, 637. ^1H NMR [500 MHz, Me_2SO-d_6] δ 9.45 (2H, d, 6.2 Hz, pyridinium 2,6), 9.03 (2H, d-like (broad), pyrrole 2,18), 9.00 (2H, d, 6.5 Hz, pyridinium 3,5), 8.98 (2H, d-like (broad), pyrrole 3,17), 8.89 (4H, s (broad), pyrrole 7,8,12,13), 8.44 (6H, d, 7.7 Hz), 8.34 (4H, d, 8.0 Hz) and 8.32 (2H, d, 7.7 Hz), (*o*- and *m*-(cyanophenyl)), 4.70 (3H, s, *N*-methylpyridinium), −2.99 (2H, s, internal pyrrole).

***cis*-$[H_2P(PhCN)_2(N\text{-}CH_3py)_2]\ (PF_6)_2$.** Anal. Calcd for $C_{46}H_{32}F_{12}N_8P_2 \cdot H_2O$: C, 54.99; N, 11.15; H, 3.41; Found: C, 54.99; N, 11.24; H, 3.32. Visible spectrum [λ, nm, in acetone (rel intens)]: 418 (1.0), 514 (0.072), 550 (0.028), 590 (0.025), 644 (0.0088). Infrared spectrum [cm^{-1}]: 2229, 1640, 1606, 1563, 1514, 1504, 1475, 1465, 1401, 1348, 1305, 1278, 1218, 1186, 1156, 1141, 1083, 1063, 1022, 997, 980, 968, 845, 805, 733, 716, 667, 636. ^1H NMR [500 MHz, Me_2SO-d_6] δ 9.47 (4H, d, 6.5 Hz, pyridinium 2,6), 9.13 (2H, s, pyrrole 17,18), 9.05 (2H, d-like, pyrrole 2,13), 9.00 (6H, d, 6.5 Hz, pyridinium 3,5 and pyrrole 3,12), 8.92 (2H, s, pyrrole 7,8), 8.44 (4H, d, 8.1 Hz) and 8.35 (4H, d, 8.1 Hz), (*o*- and *m*-(cyanophenyl)), 4.72 (6H, s, *N*-methylpyridinium), −3.01 (2H, s, internal pyrrole).

***trans*-$[H_2P(PhCN)_2(N\text{-}CH_3py)_2](PF_6)_2$.** Anal. Calcd for $C_{46}H_{32}F_{12}N_8P_2 \cdot 1\ 1/2\ H_2O$: C, 54.50; N, 11.05; H, 3.48; Found: C, 54.47; N, 11.01; H, 3.33. Visible spectrum [λ, nm, in acetone (rel intens)]: 418 (1.0), 514 (0.062), 550 (0.026), 590 (0.020), 646 (0.012). Infrared spectrum [cm^{-1}]: 2229, 1640, 1606, 1562, 1512, 1502, 1476, 1465, 1401, 1353, 1333, 1277, 1220, 1184, 1158, 1110, 1085, 1060, 1023, 999, 980, 968, 866, 846, 805, 733, 715, 667, 636. ^1H NMR [500 MHz, Me_2SO-d_6] δ 9.46 (4H, d, 6.5 Hz, pyridinium 2,6), 9.06 (4H, d-like (broad), pyrrole 2,8,12,18), 9.00 (8H, d, 6.5 Hz, pyridinium 3,5 and pyrrole 3,7,13,17), 8.44 (4H, d, 8.0 Hz) and 8.36 (4H, d, 8.1 Hz), (*o*- and *m*-(cyanophenyl)), 4.71 (6H, s, *N*-methylpyridinium), −3.02 (2H, s, internal pyrrole).

$[H_2P(PhCN)(N\text{-}CH_3py)_3](PF_6)_3$. Anal. Calcd for $C_{45}H_{35}F_{18}N_8P_3 \cdot 2\ H_2O$: C, 46.64; N, 9.67; H, 3.39; Found: C, 46.68; N, 9.65; H, 3.05. Visible spectrum [λ, nm, in acetone (rel intens)]: 420 (1.0), 514 (0.069), 550 (0.026), 590 (0.024), 646 (0.0081). Infrared spectrum [cm^{-1}]: 2230, 1642, 1607, 1570, 1561, 1514, 1463, 1401, 1354, 1332, 1278, 1218, 1184, 1159, 1093, 1059, 1022, 1000, 969, 841, 805, 732, 715, 667, 639. ^1H NMR [500 MHz, Me_2SO-d_6] δ 9.47 (6H, d, 6.6 Hz, pyridinium 2,6), 9.15 (4H, s, pyrrole 12,13,17,18), 9.07 (2H, d-like (broad), pyrrole 2,8), 9.02 (2H, d-like (broad), pyrrole 3,7), 9.00 (4H, d, 6.6 Hz) and 8.99 (2H, d, 6.6 Hz), (pyridinium 3,5), 8.44 (2H, d, 8.3 Hz) and 8.37 (2H, d, 8.3 Hz), (*o*- and *m*-(cyanophenyl)), 4.72 (9H, s, *N*-methylpyridinium), −3.05 (2H, s, internal pyrrole).

Preparation of Cobalt(II) Complexes. Cobalt(II) was inserted into the porphyrins by reacting a small excess of cobalt acetate tetrahydrate (1.2 mol equiv) and 50 to 100 mg of the porphyrin in 7.5 to 15 mL of refluxing DMF under argon for 30 min.[10] A sample of the reaction mixture in acetone ($CHCl_3$ with $H_2P(PhCN)_4$) was analyzed by visible spectroscopy. The spectrum indicated that the cobalt insertion was complete when the four Q bands of the free base (λ= 514, 550, 590, and 646 nm) collapsed to one band (λ = 530 to 532 nm). (The Soret band shifted from 420 to 410 nm with $H_2P(PhCN)_4$ but did not change with the other porphyrins). At that point, the reaction mixture was cooled in an ice−water bath for 15 min, and, in the case of $H_2(PhCN)_4$, 20 mL of chilled H_2O were added and the resulting precipitate was collected by suction filtration, washed with H_2O and MeOH, and dried to give a violet microcrystalline powder. With the various *N*-methylpyridyl porphyrins the cooled reaction solution was added dropwise to a stirred solution of 2.6 g of NH_4PF_6 in 20 mL of H_2O. The resulting precipitate was collected by suction filtration on a Buchner funnel (4−5.5-μm fritted glass disk), washed with H_2O and dried under vacuum (5 × 10^{-3} Torr, room temperature) for 48 h.

The cobalt content of the isolated samples was determined by means of quantitative controlled-potential coulometric electrolysis: First, 1.7

(31) Williams, G. N.; Williams, R. F. X.; Lewis, A.; Hambright, P. *Inorg. Nucl. Chem.* **1979**, *41*, 41.

to 2.5 mg of the cobalt(II) porphyrin were dissolved in ca. 5 mL of spectral grade DMSO (Burdick & Jackson) containing 0.1 M (TBA)-PF_6. The solution was subjected to successive electrolytic oxidation at 0.7 V followed by reduction at −0.1 V vs Ag/AgCl until the charges passed for the oxidation and the reduction cycles became approximately equal. Reticulated vitreous carbon (100 pores per inch) served as both working and auxiliary electrodes in a two-compartment cell with the compartments separated by an ultrafine fritted glass disk. Prepurified dry argon was passed through the solution in the working electrode compartment throughout the electrolysis.

Stock solutions of the porphyrins (167.5 μM) in methanol (acetone for *trans*-$[H_2P(PhCN)_2(N\text{-}CH_3py)_2](PF_6)_2$) were prepared by sonicating the desired amounts of the analyzed porphyrins in 8 mL of solvent at room temperature.

Preparation of Electrocatalysts. Porphyrins were adsorbed on the surface of pyrolytic graphite electrodes by transferring a total of 5.6-μL of freshly prepared mixtures of 100 μL of the porphyrin stock solution and 40 μL of the Nafion stock solution (sonication at room temperature was required for $[Co^{II}P(PhCN)(N\text{-}CH_3py)_3](PF_6)_3$ to keep the mixture homogeneous) to the electrode surface. The mixtures were applied by transferring several individual aliquots of ~0.2−0.5 μL and allowing the solvent to evaporate at room temperature after each application. Attempts to apply the mixtures in a single step produced coatings in which the porphyrin were more difficult to ruthenate. A background cyclic voltammogram was recorded with the coated electrode in 0.5 M NH_4PF_6−0.5 M $HClO_4$ saturated with argon. The electrode was then removed from the supporting electrolyte solution, excess liquid was taken up by a tissue leaving the electrode surface wet and the electrode was immersed in a 25 mM solution of $Ru(NH_3)_5OH_2^{2+}$. After 15 min the electrode was removed from the reaction solution, excess liquid was taken up by a tissue and the electrode was transferred to the deaerated 0.5 M NH_4PF_6−0.5 M $HClO_4$ supporting electrolyte where cyclic voltammograms were recorded. The area under the cathodic peak of the porphyrin-PhCN$Ru(NH_3)_5^{3+/2+}$ couple at ca. 0.28 V vs SCE provided a measure of the extent of the ruthenation reaction. The $Ru(NH_3)_5OH_2^{2+}$ cations which had been incorporated by the Nafion in the coatings and produced a reversible couple near −0.15 V (Figure 5A) were removed by adjusting the electrode potential to −0.4 V and rotating the electrode at 100 rpm for 1 min. If the $Ru(NH_3)_5OH_2^{2+}$ cations were not periodically removed from the coating the rate of the subsequent ruthenation step was diminished. The reason for this behavior is unclear. The entire procedure was repeated until the area under the peak at 0.28 V became constant.

Spectroscopic Measurements. UV-visible spectra were obtained with a Hewlett-Packard 8450A spectrophotometer. $CHCl_3$ (EM Science, OmniSolv) was filtered over Al_2O_3 bas. act. I (Aldrich) before use. Acetone was spectral grade (EM Science, OmniSolv). Infrared spectra were taken in KBr pellets with a Perkin-Elmer 1600 FTIR spectrometer. ^1H NMR spectra were obtained on a Bruker AM 500 spectrometer. Chemical shifts are reported in parts per million downfield of tetramethylsilane at ambient temperature.

Electrochemical Measurements. Cyclic, rotating disk, and rotating ring−disk voltammetry were carried out with a Model AFRDE5 bipotentiostat (Pine Instruments Co.) using an ASR2 rotator (Pine Instruments Co.) and an X-Y-Y′ recorder (Kipp & Zonen). Pyrolytic graphite rods (Union Carbide Co.) with the edge of the graphite planes exposed (area 0.32 cm^2) were mounted on stainless steel shafts with heat-shrinkable polyolefin tubing to construct rotating disk electrodes. The electrodes were polished on 600 grit SiC paper followed by sonication in water. The rotating pyrolytic graphite disk (0.196 cm^2) −platinum ring electrode (Model AFDTI39, Pine Instruments Co.) had a large gap (0.125 cm) between the disk and ring electrodes which facilitated the polishing of the graphite disk electrode with 600 grit SiC paper mounted on a glass rod (d = 3 mm) and the transfer of aliquots of mixtures of porphyrin and Nafion stock solutions to the graphite disk electrode without contaminating the platinum ring electrode. A thick ring electrode (0.75 cm ID, 1.0 cm OD) was employed to obtain a collection efficiency of 0.39 despite the wide gap. A conventional two-compartment electrochemical cell was employed with a platinum wire counter electrode and a saturated calomel reference electrode against which all potentials are quoted when aqueous solutions are involved. Levich currents for the reduction of O_2 at rotating disk electrodes were calculated taking the kinematic viscosity of water as 0.01 $cm^2\ s^{-1}$, the diffusion coefficient for O_2 as $1.7 \times 10^{-5}\ cm^2\ s^{-1}$ and the solubility of dioxygen in air-saturated solutions as 0.28 mM at 22 °C.

Controlled-potential electrolyses in non-aqueous solvents were carried out with a Bioanalytical Systems, Inc., Model BAS 100B instrument using a Ag/AgCl reference electrode separated from the electrolysis solution by a bridge filled with solvent and supporting electrolyte. Experiments were conducted at 22 ± 1 °C.

Acknowledgment. This work was supported by the National Science Foundation and by ONR/DARPA. We are most grateful to Dr. Yuanwu Xie for providing the simulated voltammograms shown in Figures 6 and 11. The assistance of Dr. Chaoying Rong in obtaining NMR spectra was much appreciated. Dr. Chunnian Shi generously participated in unlimited, helpful discussion.